Parallel electron-hole bilayer conductivity from electronic interface reconstruction

R. Pentcheva,[1] M. Huijben,[2] K. Otte,[1] W.E. Pickett,[3] J.E. Kleibeuker,[2] J. Huijben,[2] H. Boschker,[2] D. Kockmann,[2] W. Siemons,[2,4] G. Koster,[2] H.J.W. Zandvliet,[2] G. Rijnders,[2] D.H.A. Blank,[2] H. Hilgenkamp,[2] and A. Brinkman[2]

[1]*Department of Earth and Environmental Sciences, University of Munich, Theresienstr. 41, 80333 Munich, Germany*
[2]*Faculty of Science and Technology and MESA$^+$ Institute for Nanotechnology, University of Twente, 7500 AE, Enschede, The Netherlands*
[3]*Department of Physics, University of California, Davis, CA 95616, USA*
[4]*Department of Physics, University of California, Berkeley, CA 94720, USA*

(Dated: July 20, 2009)

Electronic reconstruction is the change in electronic properties to compensate an otherwise diverging electric potential at polar interfaces. The perovskite oxide $SrTiO_3$-$LaAlO_3$ model system illustrates the vast variety of electronic phenomena that can arise from this new type of electron doping, ranging from superconductivity to magnetic scattering. A fundamental question concerns the nature of the charge carriers and the parameters that control the electronic reconstruction. Here we show that an additional capping $SrTiO_3$ layer prevents structural or chemical reconstruction at the $LaAlO_3$ surface and provides a possibility to accommodate holes, necessary for the electronic reconstruction. By first principle calculations and transport measurements, the $SrTiO_3$ capping is found to trigger the electronic reconstruction at a significantly lower $LaAlO_3$ film thickness than for the uncapped systems. The additional capping induced temperature dependent potential shift is visualized by scanning tunneling spectroscopy. Furthermore, we provide combined theoretical and experimental evidence (from magnetotransport) for two spatially separated sheets with electron and hole carriers, that are as close as ∼1-2 nm, forming an excitingly versatile system to realize and study 2D excitonic phenomena.

The concept of electronic reconstruction [1] at the $SrTiO_3$ (STO) - $LaAlO_3$ (LAO) interface [2–4] and the resulting electronic transport properties [5–10] are based on the polar nature of LAO. The polarity of LAO arises from the LaO and AlO_2 layers being not charge neutral in the [001] direction, unlike the TiO_2 and SrO layers of STO. In the ionic limit, LaO has a charge $q = +e$ and AlO_2 $q = -e$ per unit cell. The resulting screened dipole per unit cell is $D_{screen} = q\Delta z/\epsilon$, where the spacing $\Delta z = c/2$ ($c = 3.9$ Å is the out of plane lattice parameter) and $\epsilon = 25$ is the dielectric constant of LAO [11]. Screening contributions come primarily from a strong lattice polarization of the LAO film (their contribution can be as high as $\sim 62\%$) [12]), supplemented by electronic cloud deformation [13] and finally by the presence of delocalized charges after the metal-insulator transition has taken place. For STO-LAO interfaces, the remaining screened dipole of 0.08 eÅ per cell gives rise to an internal electric field of 2.4×10^7 V/cm, and a resulting build-up of electric potential of $\Delta\phi = 0.9$ V per LAO unit cell.

This potential shift explains quantitatively why, above a threshold of 3-4 unit cells, electrons are transferred from the surface, across the LAO slab, into the STO conduction band, as shown schematically in Fig. 1a. The resulting insulator-to-metal transition has been observed experimentally for the *n*-type LaO/TiO_2-interface [6]. However, the corresponding potential shifts across LAO have not been detected so far in experiments. The potential shifts obtained from *ab-initio* calculations [12–15] are typically smaller than the suggested 0.9 V per unit cell due to effects related to the well-known underestimation of band gaps by density functional theory (DFT). For a reconstructed STO-LAO interface, it should be noted that also the LAO surface itself needs to reconstruct to avoid potential build-up, either structurally, electronically, or chemically. For electronic reconstruction one would expect holes at the surface, which has never been observed.

Here we show that an STO capping layer represents a novel pathway to tune the electronic properties of the system via an electronic reconstruction. By capping the LAO with an additional STO layer, structural and chemical reconstructions at the LAO surface are circumvented. At the same time, the O $2p$ band in the STO capping allows for hole doping, so that an exclusively electronic reconstruction mechanism comes into play. By means of the STO capping layer one enters a new regime in the field of electronically reconstructed oxide interfaces with two spatially separated 2D conducting sheets, one electron-like and the other hole-like, that can display new electronic behavior including the possibility of a 2D excitonic liquid phase.

CAPPING INDUCED INSULATOR-TO-METAL TRANSITION

The system consisting of a varying number of LAO monolayers (ML), $n = 1 - 5$ ML, and of a STO capping layer, $m = 0 - 2$ ML, stacked on an STO(001) substrate, was studied by DFT calculations in the general gradient approximation (GGA) (see Methods). The calculated

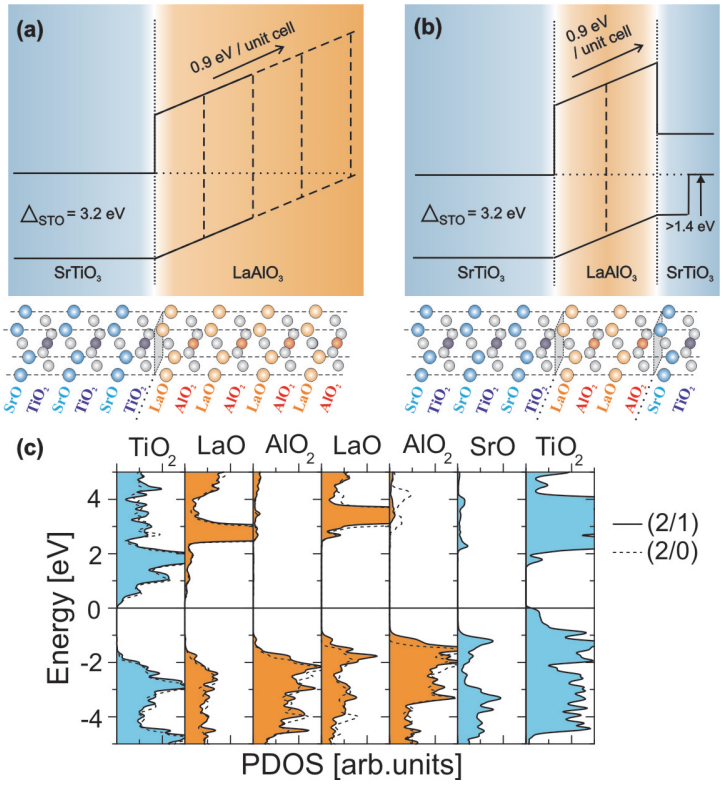

FIG. 1: **Potential build-up in polar oxides. (a)** Schematic diagram illustrating the potential build-up that arises from the polarity of 4 unit cells of LAO on a nonpolar STO substrate. Using the 0.9 eV per LAO unit cell from dipole estimates, it is expected that reconstruction occurs between 3 and 4 unit cells. **(b)** Schematic drawing of the influence of an additional capping unit cell of STO on 2 unit cells of LAO: a crucial upward shift arising from a TiO_2-derived surface band, that is not present on the LAO surface. **(c)** Layer-resolved density of states (DOS) of STO(001)/2LAO (dotted line), and STO(001)/2LAO/1STO (black line, colored area) aligned at the bottom of the Ti 3*d* band at the interface. While the O2*p*-bands in the valence band shift gradually upwards (value calculated by DFT is 0.4 V per LAO unit cell) as they approach the surface, it is the additional strong shift/broadening of the O2*p* band in the surface TiO_2 layer that closes the gap and gives rise to an electronic reconstruction.

layer-resolved densities of states are presented in Fig. 1c for 2ML LAO with and without 1ML STO capping. The effect of the electric field within the LAO film is apparent from the shifts of bands, *e.g.* by ∼0.4 eV per LAO unit cell for the uncapped system [12].

Adding a single STO capping layer is found to have a dramatic impact on the calculated electronic structure: the band gap, being 1.2 eV for STO(001)/2LAO, is nearly closed for STO(001)/2LAO/1STO. The valence band maximum is defined by the O 2*p*-states in the surface layer, while Ti 3*d*-states at the *n*-type interface mark the bottom of the conduction band. Further STO layers increase the DOS at the Fermi level (see. Suppl. Fig. S1), but have an overall weaker influence due to the lack of internal field in STO. The reduction of the band gap, and finally its closing, is due to three effects: (i) the steady upward shift of the O 2*p* states as they approach the surface [12], (ii) the band discontinuity at the interface between LAO and the capping STO layer, and (iii) a dispersive O 2*p* surface band that extends 0.8 eV above the subsurface O 2*p* band. This surface state is analogous to the one on the clean STO (001) surface [16, 17] and will be discussed in the next section. Thus, the capping layer drives the insulator-to-metal transition at an LAO thickness of only 2ML, much thinner than the critical thickness of 4ML determined in uncapped samples [6]. It also explains the metallic behavior in coupled complementary oxide interfaces with thin LAO [5]. For STO(001)/2LAO/2STO and STO(001)/3LAO/1STO (not shown here), bands overlap with a noticeable DOS at the Fermi level.

Experimentally, we confirm the crucial influence of a single monolayer of nonpolar material on the electronic interface reconstruction. STO(001)/*n*LAO/*m*STO samples were made by pulsed laser deposition of n ML of LAO and m ML of STO on TiO_2-terminated STO(001) substrates (see Methods). While uncapped STO(001)/2LAO samples are found to be insulating (sheet resistance above 1 GΩ/□), samples with an additional single ML of STO are conducting (see Fig. 2a). The conductivity is further enhanced in STO(001)/2LAO/2STO samples, but the

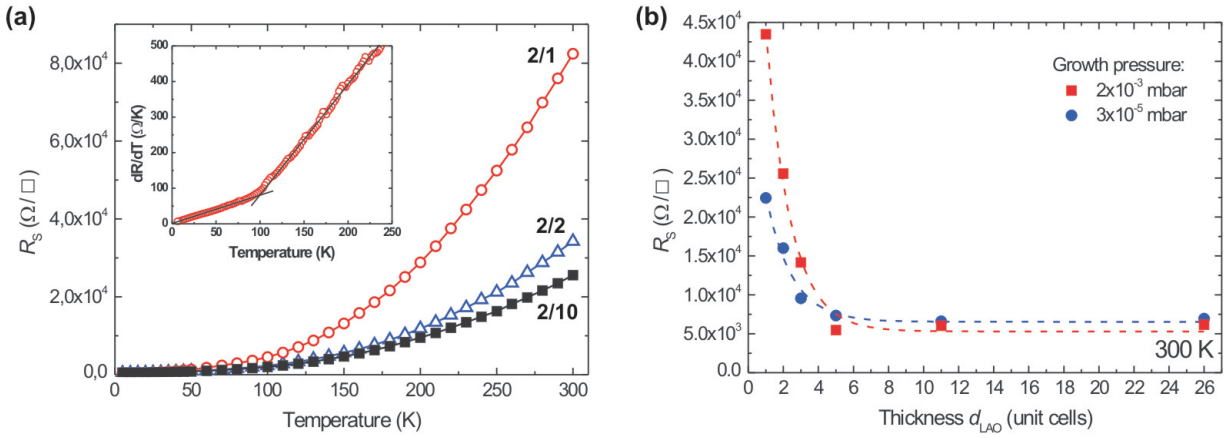

FIG. 2: **Capping induced insulator-to-metal transition.** **(a)** Sheet resistance as function of temperature for three different STO-LAO-STO samples: STO(001)/2LAO/1STO (red circles), STO(001)/2LAO/2STO (blue triangles), and STO(001)/2LAO/10STO (black squares). The sample of STO(001)/2LAO was found to be insulating. All samples are grown at 2×10^{-3} mbar of oxygen. Inset: dR/dT as function of temperature with different linear fits below and above 100 K. **(b)** Sheet resistance at room temperature of STO(001)/nLAO/10STO samples for varying n LAO interlayer thickness and a fixed number of 10 unit cells of STO capping layer. Red squares indicate samples grown at relatively high oxygen pressure (2×10^{-3} mbar), blue circles indicate samples grown at lower oxygen pressure (3×10^{-5} mbar).

influence of increasing the STO capping layer thickness weakens, as expected from the DFT results: the STO(001)/2LAO/10STO sample has almost the same conductivity as the STO(001)/2LAO/2STO sample. Samples with a single ML of LAO were found to be insulating except for the sample with a thick STO capping ($m \geq 10$).

It is known that oxygen vacancies can easily be induced in STO/LAO samples [8, 18–20]. The number of vacancies is largely determined by the growth conditions, being minimized for high oxygen deposition pressures [8, 21]. Figure 2b shows the sheet resistance for two different sets of STO-LAO-STO heterostructures with varying LAO interlayer thickness, grown at a relatively high oxygen pressure (2×10^{-3} mbar) and at lower oxygen pressure (3×10^{-5} mbar). For single-interface samples the difference in oxygen deposition pressure induces sheet resistance changes over many orders of magnitude [8]. For the coupled-interface samples, the influence of the oxygen pressure is now found to be much weaker. Apparently, the STO capping protects the underlying LAO against reconstruction via defects or adsorbates. The capping protection is promising for device application since it provides for a high level of control over the reconstruction properties and resulting carrier density. Additionally, the capping now provides a way to probe the nature of the electronic interface reconstruction, without any structural or chemical reconstruction contributions.

TUNNELING SPECTROSCOPIC EVIDENCE FOR RECONSTRUCTION

Before probing the band shifts that underlie the electronic reconstruction, it is worthwhile to understand the nature of the additional gap reduction in STO capped systems. For the uncapped case, DFT calculations have shown [12] for a few unit cells LAO on STO(001) that pronounced ionic displacements take place which counteract the bare dipole. This lattice polarization is dominated by a strong outward relaxation of the La^{3+} ions by 0.2-0.3 Å and buckling in the subsurface AlO_2 layers. In the surface AlO_2 layer both cations and anions relax inwards by similar amounts, leading to a vanishing contribution to the dipole moment.

This relaxation pattern changes drastically when a capping layer is added (see Suppl. Fig. S2 for more details): while the surface AlO_2-layer in the uncapped systems shows negligible polarization, the surface TiO_2-layer in the capping STO layer buckles with $z_{\mathrm{Ti}} - z_{\mathrm{O}} \approx -0.15$ Å, leading to a strong dipole moment in the layer of -0.50 eÅ (having the same sign as the bare dipole moment). However, the subsurface SrO layer shows a positive polarization. So, effectively, the net contribution of the TiO_2 and SrO layers does not affect appreciably the total ionic dipole moment of the film (which scales with the number of LAO layers), and the gap reduction cannot be explained by this difference in ionic displacements.

In fact, it is an electronic state at the STO surface that is responsible for the energy shift. The evolution

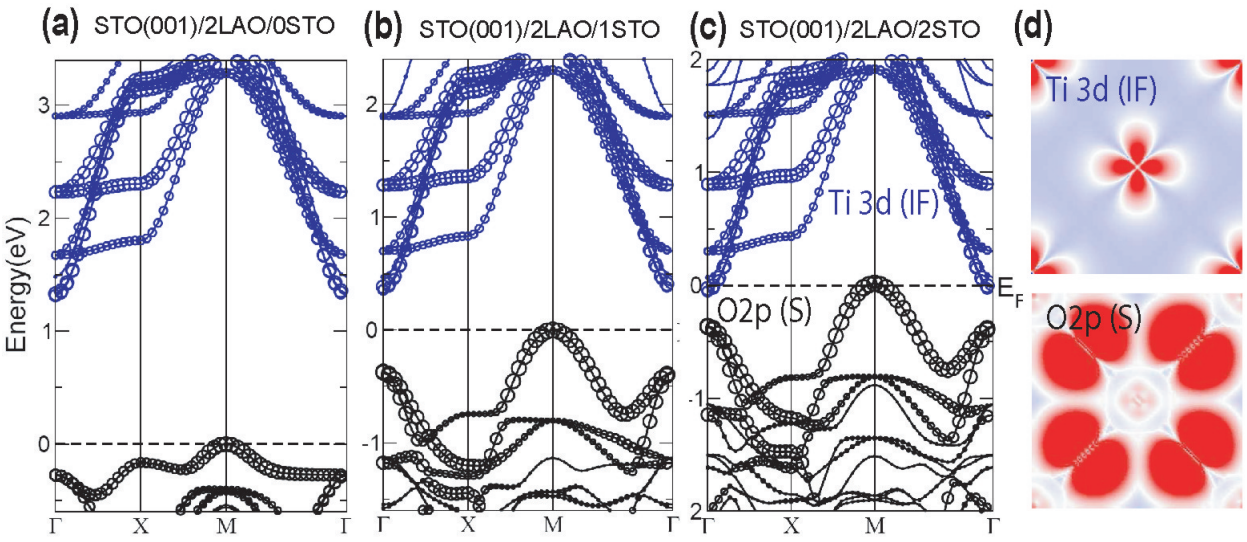

FIG. 3: **Electron and hole bands. (a-c)** Influence of the STO capping on the band structure of STO(001)/2LAO/mSTO with increasing number of capping layers ($m = 0 - 2$), showing the closing of the band gap due to overlap between surface O $2p$ states (black circles) and interface Ti $3d$ states (blue circles). **(d)** The electron density distribution in the TiO_2 layers of the $m = 2$ sample shows at the interface electrons in the Ti $3d_{xy}$ orbitals (top) and holes in the O $2p_\pi$ bands at the surface (bottom). The electron density is integrated between -0.6 and 0.0 eV.

of the band structure of STO(001)/2LAO/mSTO with increasing number of capping layers ($m = 0 - 2$) is depicted in Fig. 3. In the capped systems a dispersive O $2p$ surface band extends 0.8 eV above the subsurface O $2p$ band and effectively reduces the band gap of STO. Consequently, the reconstruction takes place for thinner LAO layers than in the uncapped case (see Fig. 1b). We note that this band has its maximum at the M(π,π)-point, while the bottom of the Ti $3d$ conduction band is at Γ, resulting in an indirect band gap. The implications of this finding will be discussed in the following.

The STO(001)/2LAO/1STO sample, theoretically being on the verge of reconstruction, is expected to show appreciable band shifts as a function of temperature. In analogy to $BaTiO_3$, it is expected [17] that the upward shift is largest at temperatures below the cubic-to-tetragonal transition at 105 K [22]. This new temperature dependent ingredient to the electronic interface reconstruction makes it now possible to experimentally visualize the band shifts that are required in the reconstruction scenario.

We have performed scanning tunneling microscopy (STM) and spectroscopy (STS) on oxide samples with electronically reconstructed interfaces. The STM was performed in ultra high vacuum using a variable temperature cryostat. Figure 4 shows the current-voltage tunneling characteristics of a STO(001)/2LAO/1STO sample and the derived normalized conductivity $(dI/dV)/(I/V)$, which can be interpreted as the sample local density of states (LDOS). At room temperature, the Fermi energy lies within a small band gap. At 77 K, the band gap is larger and the Fermi energy has shifted to the conduction band.

Assuming that tunneling occurs both to the surface and to the substrate-LAO interface, these spectroscopic features can be understood on the basis of the band structure calculations (as shown in Fig. 3). The small gap observed at 300 K is consistent with the idea that the upward shift of the STO surface valence band around the M-point is not yet large enough for reconstruction (see Fig. 3b). The gap lies between the valence band at the M-point in the surface and the conduction band at the Γ-point in the substrate-LAO interface. At 77 K, where the M-point valence band upward shift is expected to be larger (since $T < 105$ K), the Fermi energy is indeed found to lie in the conduction band of the substrate-LAO interface, indicating that electronic reconstruction has taken place, as displayed schematically in Fig. 4b.

The substantial increase of the STS band gap when cooling down from room temperature to 77 K can be understood from an analysis of measurements of the tunnel current, I, versus the tip-sample separation, z, at fixed (negative) sample bias. The tunnel current $I \propto e^{-2\kappa z}$ is measured at negative sample biases in the range from -1 V to -3 V. The inverse decay length, κ, is substantially larger at room temperature ($\sim$ 80 %) than at 77 K. The inverse decay length is given by $\kappa = \sqrt{C + k_\parallel^2}$, where C only depends on the temperature independent tunnel barrier height and $k_\parallel$ is the parallel momentum of the surface electronic structure [23]. The relatively large κ at room temperature strongly supports the idea that

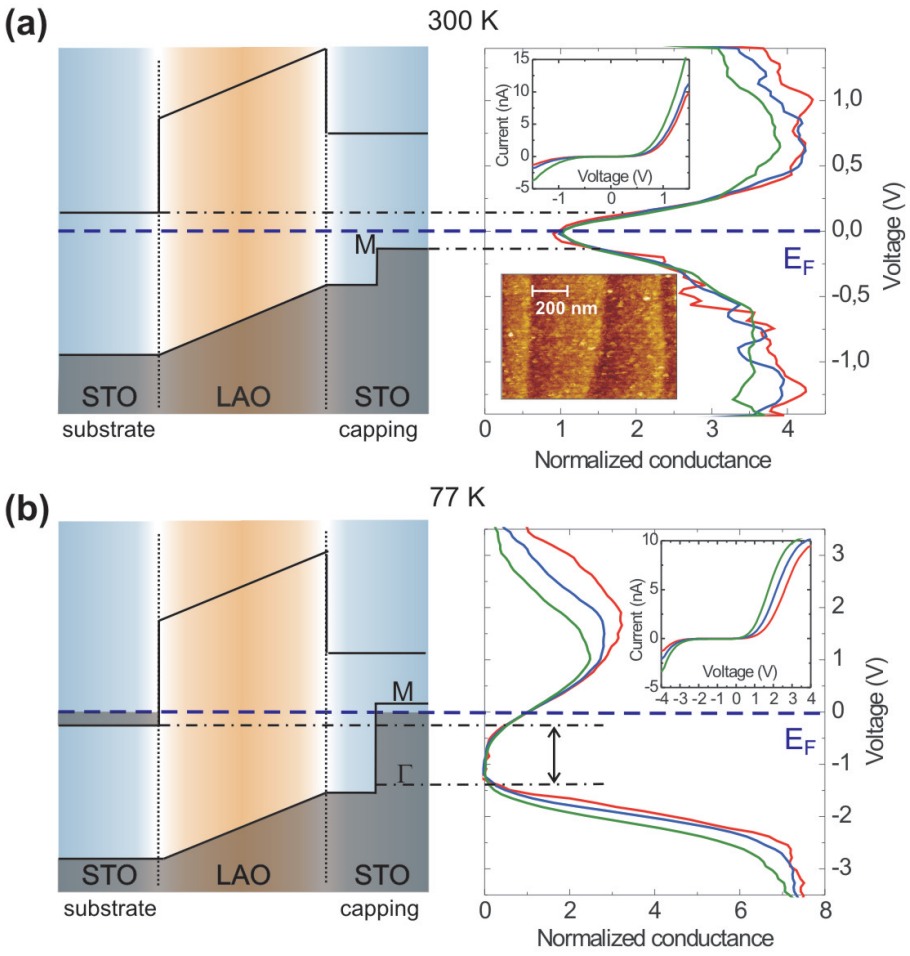

FIG. 4: **Scanning tunneling spectroscopy.** **(a)** STM normalized conductance $(dI/dV)/(I/V)$ measurements of a STO(001)/2LAO/1STO sample at 300 K for different tip-sample distances (current set-point respectively 1.5 nA, 2.0 nA, and 4.0 nA at a bias voltage of -1.5 V). The schematic drawing explains the small 0.5 eV gap between the valence band at the M-point of the STO capping surface and the conduction band at the substrate-LAO interface. The Fermi energy, E_F, at $V = 0$ V (blue dashed line) lies in the gap. The upper inset shows the current-voltage characteristics from which the conductance was derived and the lower inset shows an STM topography image taken at 300 K with a bias voltage of -1.0 V. **(b)** Normalized conductance at 77 K (current set-point respectively 1.5 nA, 2.5 nA, and 4.0 nA at a bias voltage of -4.0 V). The schematic drawing explains the 1.5 eV gap between the valence band Γ point at the STO capping surface and the substrate-LAO interface conduction band. The Fermi energy (blue dashed line) lies now in the conduction band. Band bending is not depicted on this scale. The inset shows the current-voltage characteristics.

at room temperature tunneling occurs from filled surface electronic states with a nonzero parallel momentum (*i.e.* regions near the M point of the surface Brillouin zone) to empty states of the tip. Accordingly, at 77 K tunneling mainly occurs from filled electronic states near the Γ point of the surface Brillouin zone to empty states of the tip, leading to substantial increase of the measured band gap. The latter analysis emphasizes that the electrons that are transferred across the STO/LAO/STO structure upon reconstruction originate from the M point of the surface STO Brillouin zone.

PARALLEL ELECTRON-HOLE BILAYER CONDUCTIVITY

The calculated electron density distribution in Fig. 3d displays electrons of Ti $3d_{xy}$ orbital character in the interface TiO_2 layer, while holes of O $2p_\pi$ type are present in the surface TiO_2 layer. Experimentally it has been confirmed in single interface STO/LAO samples that the lowest lying Ti states are of Ti $3d_{xy}$ character [24], while holes have not been observed yet in any STO/LAO interface sample.

To investigate the possibility of a parallel electron-hole

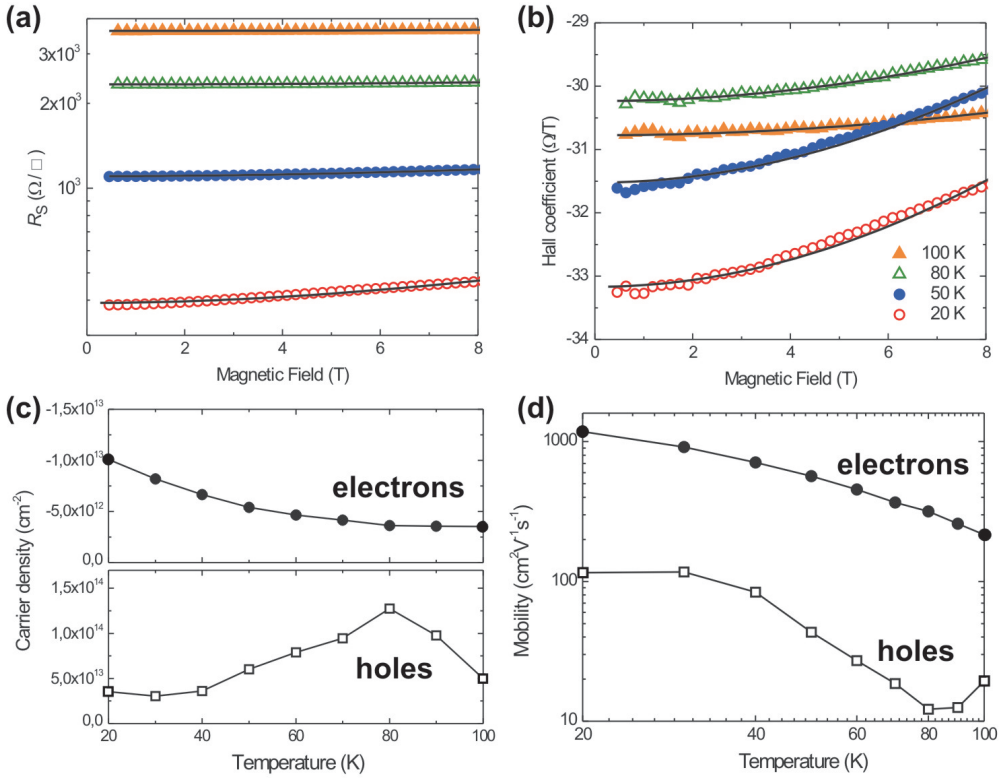

FIG. 5: **Magnetoresistance effects from two-band conductivity.** **(a)** Sheet resistance as function of magnetic field at different temperatures for a STO(001)/2LAO/1STO sample, exhibiting a positive magnetoresistance. **(b)** Hall coefficient (R_H/H) of the same sample as a function of magnetic field. **(c)** Sheet carrier densities and **(d)** mobilities as obtained from a two-band fit to the magnetoresistance and Hall data at each temperature.

bilayer and the sign of the charge carriers in capped systems, magnetoresistance and Hall data were analyzed. All conducting STO/LAO/STO samples display a positive non-quadratic magnetoresistance and a Hall resistance whose slope increases for higher fields. An example is given in Fig. 5. Quantum oscillations can still be excluded because of the low mobility. Neither is there any signature of a negative magnetoresistance contribution that occurs for single-interface samples deposited at high oxygen pressure [8]. It is, therefore, natural to interpret the observations in terms of multiband conductivity. Indeed, in the temperature range up to 100 K, the magnetoresistance as well as the Hall resistance can be fitted (solid lines in Fig. 5 a and b) with a two band model (see Supplementary Information). The two carrier concentrations and two mobilities could be obtained from fitting as a function of temperature. The results for the STO(001)/2LAO/1STO sample are shown in Fig. 5 c and d.

The positive carrier sign of one of the bands at low temperatures indicates hole-type conductivity for one band, while the other band is of electron-type. For equal signs of the two carrier densities, no fit to the data could be obtained. Neither oxygen vacancy doping, nor doping by cation substitution, have ever been shown to give rise to hole conductivity in the STO/LAO system. Based on the predicted conductivity contribution of the O $2p_\pi$ surface band of STO(001)/2LAO/1STO samples (Figs. 3 b and d), we attribute the hole band to the surface. The electron band, with a lower carrier density but a much larger mobility, is naturally attributed to the Ti $3d_{xy}$ band at the interface to the substrate. Note, that the hole density is about an order of magnitude larger than the electron density. However, the Hall effect is dominated by the electron band because of its large mobility. The unequal number of electrons and holes illustrates that not all charge carriers are visible in transport measurements.

Neither magnetoresistance, nor a nonlinear Hall resistance are observed above 100 K. While at these high temperatures the mobilities become so low that no magnetoresistance effects are expected anyway ($\mu^2 H^2 << 1$ in the two-band equations as described in the Supple-

mentary Information), the disappearance of the two-band effects around 100 K is in excellent agreement with the STS data, with the $R_S(T)$ behavior changing around 100 K (see the inset of Fig. 2a), and with the theoretical expectations.

The sensitivity of the band overlap to the screened potential build-up is exemplified by increasing either the number of LAO interlayer unit cells or the number of unit cells in the STO capping layer. For thicker LAO and thicker STO (a large number of samples with varying numbers of unit cells of LAO and STO capping have been analyzed, see Suppl. Fig. S3), the conductivity at the surface is found to be of electron-type over the entire temperature regime.

DISCUSSION

As shown in the band structure of $m = 0-2$ STO(001)/2LAO/mSTO in Fig. 3, the gap closes because the top of the surface O $2p$ band overlaps with the Ti $3d$ conduction bands at the interface; this occurs in the calculation just around the STO(001)/2LAO/1STO system. Experimentally, we find indeed from the STM and magnetotransport data that reconstruction takes place in the STO(001)/2LAO/1STO, and that this happens below $\sim$ 100 K. However, at $T > 100$ K conductivity also occurs, suggesting that some amount of additional carriers (e.g. from thermal excitations, vacancies, cation interdiffusion, etc.) are already present at the interface (the confinement being due to band bending) before reconstruction has taken place. The crossover from having pre-existing carriers to having reconstruction can be seen as well in the inset of Fig. 2a, where the difference in slope in the resistivity versus temperature is shown.

The STO capping has enabled us to show that holes are present in reconstructed oxide interface samples. The mobility is low and it is expected that the holes can become localized or eliminated in uncapped STO/LAO systems much more strongly (*e.g.* by absorbed molecules or by ionic surface reconstruction). This possibly explains the large sensitivity of uncapped samples to growth conditions and the possibility to manipulate the interface conductivity by an atomic force microscope tip [25, 26].

The surface valence band has its maximum at the M=(π,π) zone corner, whereas the substrate-LAO interface conduction band has its minimum at the zone center. This makes the band overlap distant not only in real space (across 12 Å or more, depending on capping layer thickness) but also indirect in momentum. As a practical consequence, an electron at the surface cannot move to the substrate without some mechanism to supply the momentum transfer. The obvious mechanism is via phonons, specifically M=(π,π) phonons. These are zone boundary optical phonons, which typically lie at a few tens of meV energy. Equilibration of electrons and holes across the LAO slab will be slow at low temperature, but will occur rapidly as soon as optical phonons are excited.

A further consequence of this 2D electron-hole bilayer is that it provides the conditions necessary for formation of a 2D excitonic liquid [27, 28] comprised of interacting indirect excitons. The excitonic condensate has long been studied theoretically, but without a great deal of strong evidence of its occurrence in practice. In this oxide nanostructure the separation of the 2D electron and hole gases can be varied by the choice of polar material as well as capping material. Furthermore, the carrier densities can be tuned by gating, allowing a substantial parameter range to be probed.

METHODS

Sample growth The heterostructures used in this study were grown epitaxially using pulsed laser deposition from single crystal LAO and STO targets on TiO_2-terminated STO(001) substrates [29], as described previously in Refs. 5 and 8. The growth was monitored in-situ by RHEED analysis [30], allowing precise thickness control of the LAO and STO layers at the unit cell scale and accurate characterization of the growth dynamics. The observed intensity oscillations indicated clearly a layer-by-layer growth mode with a very smooth surface. After growth, the sample was slowly cooled down to room temperature in oxygen at the deposition pressure. A smooth surface morphology and correct crystal structure of the final heterostructures were confirmed by atomic force microscopy and x-ray diffraction.

DFT details The DFT calculations were performed with the full-potential linear augmented plane wave (FP-LAPW) method in the WIEN2k implementation [31]. The generalized gradient approximation (GGA) [32] of the exchange and correlation potential is used. Because the studied systems do not show a noteworthy occupation of the Ti $3d$ band, including a Hubbard U term within GGA+U [33] is not expected to affect the results.

LAO films with $n = 1-3$MLs on STO(001) covered by a capping STO layer of $m = 0-2$ MLs are modeled in the supercell geometry with two inversion symmetric surfaces on both sides of the slab to avoid spurious electric fields. The slabs are separated in z-direction by a vacuum of 10-12 Å in order to minimize interactions between the periodic images. The lateral lattice constant is set to the GGA value (3.92 Å), slightly larger than the experimental lattice parameter 3.905 Å of bulk STO. Thus the LAO ($a = 3.79$ Å) is subject to 3% tensile strain. 21 **k**-points are used in the irreducible part of the Brillouin zone and a full structural optimization was performed within the tetragonal unit cell. For further details on the calculation see Ref. [12].

ACKNOWLEDGMENTS

This work is financially supported by the Dutch Foundation for Fundamental Research on Matter (FOM), the Netherlands Organization for Scientific Research (NWO) through VIDI and VICI grants, NANONED, the Bavaria-California Technology Center (BaCaTeC), DOE's Computational Materials Science Network, DOE Grant DE-FG03-01ER45876, and a grant for computational time at the supercomputer HLRBII at the Leibniz Rechenzentrum.

[1] Hesper, R., Tjeng, L. H., Heeres, A. & Sawatzky, G. A. Photoemission evidence of electronic stabilization of polar surfaces in K_3C_{60}. *Phys. Rev. B* **62**, 16046 (2000).

[2] Ohtomo, A. & Hwang, H. Y. A high-mobility electron gas at the $LaAlO_3/SrTiO_3$ heterointerface. *Nature* **427**, 423–426 (2004).

[3] Ohtomo, A. & Hwang, H. Y. Corrigendum: a high-mobility electron gas at the $LaAlO_3/SrTiO_3$ heterointerface. *Nature* **441**, 120 (2006).

[4] Nakagawa, N., Hwang, H. Y. & Muller, D. A. Why some interfaces cannot be sharp. *Nature Mater.* **5**, 204–209 (2006).

[5] Huijben, M. *et al.* Electronically coupled complementary interfaces between perovskite band insulators. *Nature Mater.* **5**, 556–560 (2006).

[6] Thiel, S., Hammerl, G., Schmehl, A., Schneider, C. W. & Mannhart, J. Tunable quasi-two-dimensional electron gases in oxide heterostructures. *Science* **313**, 1942–1945 (2006).

[7] Reyren, N. *et al.* Superconducting interfaces between insulating oxides. *Science* **317**, 1196 (2007).

[8] Brinkman, A. *et al.* Magnetic effects at the interface between non-magnetic oxides. *Nature Mater.* **6**, 493–496 (2007).

[9] Caviglia, A. D. *et al.* Electric field control of the $LaAlO_3/SrTiO_3$ interface ground state. *Nature* **456**, 624–627 (2008).

[10] Basletić, M. *et al.* Mapping the spatial distribution of charge carriers in $LaAlO_3/SrTiO_3$ heterostructures. *Nature Mater.* **7**, 621 (2008).

[11] Hayward, S. A. *et al.* Transformation processes in $LaAlO_3$: neutron diffraction, dielectric, thermal, optical, and Raman studies. *Phys. Rev. B* **72**, 054110 (2005).

[12] Pentcheva, R. & Pickett, W. E. Avoiding the polarization catastrophe in $LaAlO_3$ Overlayers on $SrTiO_3$ (001) through polar distortion. *Phys. Rev. Lett.* **102**, 107602 (2009).

[13] Ishibashi, S. & Terakura, K. Analysis of screening mechanisms for polar discontinuity for $LaAlO_3/SrTiO_3$ thin films based on ab initio calculations. *J. Phys. Soc. Jpn.* **77**, 104706 (2008).

[14] Chen, H., Kolpak, A. M. & Ismail-Beigi, S. Fundamental asymmetry in interfacial electronic reconstruction between insulating oxides: An ab initio study. *Phys. Rev. B* **79**, 161402 (2009).

[15] Son, W., Cho, E., Lee, B., Lee, J. & Han, S. Density and spatial distribution of charge carriers in the intrinsic n-type $LaAlO_3$-$SrTiO_3$ interface. *Phys. Rev. B* **79**, 245411 (2009).

[16] Kimura, S., Yamauchi, J., Tsukada, M. & Watanabe, S. First principles study on electronic-structure of the (001) surface of $SrTiO_3$. *Phys. Rev. B* **51**, 11049 (1995).

[17] Padilla, J. & Vanderbilt, D. Ab initio study of $SrTiO_3$ surfaces. *Surf. Sci.* **418**, 64–70 (1998).

[18] Siemons, W. *et al.* Origin of charge density at LaAlO3 on SrTiO3 heterointerfaces: possibility of intrinsic doping. *Phys. Rev. Lett.* **98**, 196802 (2007).

[19] Herranz, G. *et al.* High mobility in $LaAlO_3/SrTiO_3$ heterostructures: origin, dimensionality, and perspectives. *Phys. Rev. Lett.* **98**, 216803 (2007).

[20] Kalabukhov, A. *et al.* Effect of oxygen vacancies in the $SrTiO_3$ substrate on the electrical properties of the $LaAlO_3/SrTiO_3$ interface. *Phys. Rev. B* **75**, 121404 (2007).

[21] Huijben, M. *et al.* Structure-property relation of $SrTiO_3/LaAlO_3$ interfaces. *Adv. Mater.* **21**, 1665–1677 (2009).

[22] Padilla, J. & Vanderbilt, D. Ab initio study of $BaTiO_3$ surfaces. *Phys. Rev. B* **56**, 1625–1631 (1997).

[23] Zandvliet, H. J. W. & van Houselt, A. Scanning Tunneling Spectroscopy. *Ann. Rev. Anal. Chem.* **2**, 37–55 (2009).

[24] Salluzzo, M. *et al.* Orbital reconstruction and the two-dimensional electron gas at the $LaAlO_3/SrTiO_3$ interface. *Phys. Rev. Lett.* **102**, 166804 (2009).

[25] Cen, C. *et al.* Nanoscale control of an interfacial metal–insulator transition at room temperature. *Nature Mater.* **7**, 298–302 (2008).

[26] Cen, C., Thiel, S., Mannhart, J. & Levy, J. Oxide Nanoelectronics on Demand. *Science* **323**, 1026–1030 (2009).

[27] Keldysh, L. V. & Kopaev, Y. V. Possible instability of the semimetal state toward coulomb interaction. *Sov. Phys. JETP* **6**, 2219 (1965).

[28] des Cloizeaux, J. Exciton instability and crystallographic anomalies in semiconductors. *J. Phys. Chem. Solids* **26**, 259–266 (1965).

[29] Koster, G., Kropman, B. L., Rijnders, A. J. H. M., Blank, D. H. A. & Rogalla, H. Quasi-ideal strontium titanate crystal surfaces through formation of Sr-hydroxide. *Appl. Phys. Lett.* **73**, 2020–2022 (1998).

[30] Rijnders, A. J. H. M., Koster, G., Blank, D. H. A. & Rogalla, H. In situ monitoring during pulsed laser deposition of complex oxides using reflection high energy electron diffraction under high oxygen pressure. *Appl. Phys. Lett.* **70**, 1888–1890 (1997).

[31] Blaha, P., Schwarz, K., Madsen, G. K. H., Kvasnicka, D. & Luitz, J. WIEN2k. *(Karlheinz Schwarz, Techn. Univ. Wien, Austria), ISBN 3-9501031-1-2* (2001).

[32] Perdew, J. P., Burke, K. & Ernzerhof, M. Generalized gradient approximation made simple. *Phys. Rev. Lett.* **77**, 3865–3868 (1996).

[33] Anisimov, V. I., Solovyev, I. V., Korotin, M. A., Czyzyk, M. T. & Sawatzky, G. A. Density-functional theory and NiO photoemission spectra. *Phys. Rev. B* **48**, 16929–16934 (1993).